Electrostatic tuning of transmission in NbS_2/WSe_2 2D Lateral Hetero-Structures: A computational study

Poonam Kumari[1], Zahra Golsanamlou[1], Alexander Smogunov[2], Luca Sementa[1,*], Alessandro Fortunelli[1,*]

[1] CNR-ICCOM and IPCF, Consiglio Nazionale delle Ricerche, via G. Moruzzi 1, Pisa 56124, Italy

[2] SPEC, CEA, CNRS, Université Paris-Saclay, CEA Saclay, Gif-sur-Yvette Cedex, 91191 France

Abstract

We present a first-principles computational study of the NbS_2/WSe_2 junction between two transition metal dichalcogenide monolayers as a prototypical metal/semiconductor 2-dimensional (2D) lateral hetero-structure (LH) to investigate the effects of electrostatic perturbations on electron transport in 2D LH systems. In order to simulate electrostatic (charged or dipolar) defects in the substrate, we introduce ionic systems (LiF lines) properly positioned in two different configurations and study cases, corresponding to modeling two different phenomena: (i) an electrostatic defect in the middle of the semiconducting part of the hetero-structure (qualitatively analogous to a gate voltage opposing transmission), and (ii) an electrostatic perturbation re-aligning and flattening the electrostatic potential along the asymmetric LH junction. In the former case, we determine a substantial decrease of transmission even for small values of the perturbation (providing information that can be used to achieve a quantitative correlation between substrate-induced defectivity and device performance degradation in experiment), whereas in the latter we predict that electron transport can be significantly enhanced by properly tuning external electrostatic perturbations at the interface.

* Corresponding authors' emails: alessandro.fortunelli@cnr.it (AF), luca.daumann@gmail.com (LS)

Introduction

Two-dimensional materials (2DMs) have gained significant attention in recent years owing to their novel properties which can be harnessed for potential applications in electronic and optoelectronic devices [1-3]. Among these, transition metal dichalcogenides (TMDs), which are layered Van der Waals (vdW) materials, form an important class, with members ranging from metals, semimetals to semiconductors [4-6]. The weak vdW forces between the layers in these materials allow exfoliation of thin films with stoichiometry MX_2 (with M the transition metal and X the chalcogen atoms) up to monolayer thickness [7-9].Promising for applications is then to combine different types of TMDs with varying properties (such as metal/semiconductor) to form lateral (LH) or vertical (VH) hetero-structures [10-12] which offers an appealing way to modulate electron transport at a fundamental level in optoelectronic devices [13-14]ideally down to sub-5nm miniaturization [15]. As a result, a wealth of studies has appeared on TMD LHs and VHs both at the experimental [16-20] and theoretical levels [21-25].

As a drawback in this approach, the same ultrathin size that make 2DMs appealing for applications also entails that the properties of these systems are liable to atomistic fluctuations to a degree much higher than mesoscopic systems. In this respect, the substrate on which 2DMs are supported can play a critical role in generating defects that deteriorate the response (optical, band structure, transmission) of 2DMs. A paradigmatic comparison of photoluminescence spectra of monolayer MoS_2 freestanding and supported on a Si/SiO_2 substrate showed that the freestanding peak shows a blue shift as well as increased intensity compared to the supported system [26]. Qualitatively similar findings were reported for other TMDCs: e.g., for WSe_2 in a recent study comparing the photoluminescence spectra of suspended WSe_2 with that of WSe_2 grown on a silica substrate [27]. Other studies found similar effects, with ideal performance only achieved in the absence of the substrate [28-31]. Basically two mechanisms have been invoked to rationalize these effects. One source of defects has been singled out in the high-temperature CVD growth process, that can produce chemical anchoring of the 2D phase onto the substrate, whence an induced *strain* upon cooling which affects the optical gap and the conductance of 2D MoS_2 [32]. A different type of defects are *vacancies* produced by imperfectly controlled growth, in the form of both chalcogen vacancies [33] as well as transition metal vacancies [34], with the substrate itself again playing a role in stabilizing these other defects [35]. Note that anion vacancies are

often neutral [36, 37, 38], whereas cation vacancies are typically charged. Other common defects in oxide materials can be associated with interstitials, which can give rise to dipolar electric fields, or more extended defects such as grain broundaries, which can also host charged or dipolar species. However, despite the insight gained from these studies, a quantitative correlation between substrate-induced defectivity and device/materials performance degradation has not been drawn so far. On the opposite, a survey of available data suggests that strain induced by chemical anchoring onto the substrate and neutral vacancies cannot always justify the loss of performance with respect to ideal monolayers [31].

To fill this gap and provide alternative mechanisms to rationalize the observed non-idealities, here we explore the hypothesis that, in addition to previously identified mechanisms, electrostatic phenomena, in particular electrostatic perturbations associated with substrate defects, can play a role in modulating electron transport (transmission) in these systems. Considering that ionic (i.e., to some extent charge-separated) supports, such as oxides, are typically used for growing 2D materials, this hypothesis seems worth exploring. The type of defects usually assumed to be dominant in oxide supports, i.e., charge traps in the substrate, generate an electrostatic field in which dipolar or quadrupolar components will be dominant. These charge defects are not well characterized experimentally, so that we do not have a precise atomistic model for these defects except that they are known to affect conductance although buried in the substrate, which implies that they must have a long-range effect, thus they must be associated with electrostatic perturbations. Studies have been reported showing the presence of charged traps in the substrate. For example, Y. Guo at. al [39] studied the charge trapping at MoS_2-SiO_2 interfaces and studied the impact of the trapped charges on the carrier transport. They concluded that the trapped charges give rise to unscreened Coulomb scattering. Charge traps also results in variable range hopping in the carrier transport of MoS_2 sheets. However, detailed theoretical studies of the effect of such charge traps are absent in the literature. Here, we conduct a proof-of-principle computational study on this topic. Our goal is to identify the principles governing substrate electrostatic effects on transport in 2DMs in general, so that we can control them. We will also investigate if it is possible to tune them to ideally optimize, rather than destroy, conductance.

To this end, we focus on a NbS_2/WSe_2 metal/semiconductor LH, as a prototypical example to investigate and understand conductance mechanisms, modeled at the Quantum-Mechanical (QM) level. NbS_2 is one of the most investigated metallic dichalcogenides. For the semiconducting part we selected WSe_2, as a representative of semiconducting TMDs. We underline the similarity in electronic properties of WSe_2 with the most studied semiconducting TMDC, i.e., MoS_2: they are both semiconductors with qualitatively similar atomistic structure (apart from the difference in lattice parameter) and very similar electronic structures, both of them being direct bandgap material at the monolayer limit with a bandgap of 1.90 eV and 1.65 eV respectively [40]. Moreover, the NbS_2/WSe_2 LH has the advantage of presenting very little lattice mismatch between the component monolayer phases (see the discussion below). This helps us to separate the electrostatic phenomenon that we are investigating from other possible phenomena, originating from structural diversity and strain or from doping effects governing LH interfaces for TMDC pairs with large lattice mismatch such as NbS_2/MoS_2 [41]. By selecting a system with no lattice mismatch we have two clean interfaces and we can investigate electrostatic effects in pure form. Finally, note that in a previous study, we have analyzed the NbS_2/WSe_2 LH in detail and derived quantitative modeling of electron transport. We found it to be a promising system for potential applications, such as FET, since e.g. stoichiometric fluctuations stabilize the system without deteriorating its electronic features [42-43]. For these reasons, we consider NbS_2/WSe_2 as an ideal system to investigate defect modelling. We introduce an electrostatic perturbation in the form of LiF chains as a mean of producing a quadrupolar field which is compatible with our 3D periodic approach. The actual nature of defects in oxides and the perturbations caused by them are not known with certainty. In the literature it has been claimed that defects are associated with vacancies, or localized point defects [44]. It has also been claimed that isolated vacancies are prone to aggregate into small clusters with different geometries [45]. Finally, extended defects such as grain boundaries do exist, although their effect has not been definitively ascertained, to the best of our knowledge, due to the difficulties in characterizing these structures. A line defect model gives rise to an electrostatic field perturbation, which should not be qualitatively different from that produced in all these cases. This is clear in the case of spatially extended defects such as grain boundaries or clusters of point defects, whose electrostatic perturbation will necessarily have a long-range extension. Additionally, our modeling should be at least qualitatively correct also in the case of localized point defects, if the

electrostatic perturbation associated with them is spatially wide enough to affect all the conducting paths in a sizeable region of the system. Indeed, we will see later that the effect of the line of defects is long-ranged also in the transmission direction (see the electrostatic potential profiles below), implying that the size of the electrostatic perturbation associated with a localized defect is larger than the y-lattice parameter of our system, thus justifying our modeling of localized defects as periodic. Technically, note finally that, due to periodic boundary conditions in our plane-wave code, we cannot introduce a dipolar perturbation (the energy would diverge [46]), so we introduce a quadrupolar perturbation (simply producing a shift in the electrostatic background [46]) by symmetrizing the LiF dipolar perturbation putting it above and below the LH monolayer.

We focus on two phenomena. First, we use the LiF electrostatic perturbation as a model of charged defects in the substrate with a polarity opposing conductance. We demonstrate that even a modest perturbation can dramatically deteriorate the transmission properties of the 2D LH, and we rationalize this finding via an electrostatic potential alignment and a fragment analysis of the electrostatic potential. As discussed in Section 3, our predictions compare qualitatively well with and are supported by the experimental studies in the literature focusing on the effect of the substrate and its defects on degrading the ideal properties of TMD monolayers [27,30, 47, 48, 49]. With this rationale in hand, we then explore whether properly tuned electrostatic effects can be used to improve rather than deteriorate transmission. Indeed, we identify a defect configuration next to the LH interface which improves the electrostatic potential alignment, and thus the transmission profile, and thus conductance, thus making the LH more robust and suitable for potential applications. Despite the limitations of the present proof-of-principle study, here we start exploring the effect of an electrostatic perturbation on transmission, quantitatively, and we show which phenomena we can encounter and provide some quantitative estimates, thus making progress toward a quantitative modeling of the effect of electrostatic perturbations on transmission.

2. Methodology

Electronic structure and geometric optimizations were carried out via first-principles density-functional theory (DFT) as implemented within the Quantum Espresso (QE) package

[50-51]. A vacuum of 20 Å was used to minimize the interactions due to replicas of the unit cells. A plane-wave basis set, a scalar-relativistic ultrasoft pseudopotentials and a gradient-corrected exchange-correlation (xc-)functional (the Perdew-Burke-Ernzerhof, PBE [52]) were used. Monkhorst-Pack k-meshes of 1 × 20 × 1 were used to sample the Brillouin zone (BZ). An energy cut-off of 40 Ry for the selection of plane-wave basis set to describe the wave function and 400 Ry for the electron density were used. The DFT band structure was then analyzed to derive Hamiltonians based on maximally localized Wannier functions via the Wannier90 code, [53-54] using transition-metal d-orbitals and chalcogenide p-orbitals in the basis set. More details about Wannier90 are given in the Supporting Information (Figures S6-S9). After obtaining the Wannier Hamiltonian, we used a home-made code based on non-equilibrium Green's functions to obtain transmission coefficients. Transmission was calculated using 44 k-points in the planar direction (Y).

3. Results and discussion

An atomistic model for the NbS_2/WSe_2 LH was created. First, we took monolayers of NbS_2 and WSe_2 at the experimental lattice constants of 3.344 Å and 3.319 Å, respectively [55]. After full geometric relaxation using DFT, the lattice constants obtained were 3.346 Å and 3.323 Å, respectively. With these two unit cells a system with 4 NbS_2 unit and 4 WSe_2 unit was built at an intermediate lattice constant of 3.331 Å. The dynamic stability of the system was confirmed via Ab Initio Molecular Dynamics simulations whose results are presented in the SM (Figure S1). The structures in Figure. 1 were considered as the scattering regions connected on both sides to semi-infinite NbS_2 electrodes.

Previously, we derived quantitative modeling of electron transport in the NbS_2/WSe_2 metal/semiconductor junction, and found it to be a promising system for potential applications, since e.g. stoichiometric fluctuations stabilize the system without deteriorating its electronic features [42-43]. To perturb the conductance of this system within an electrostatic scenario, we introduce electrostatic defects, with the goal of modelling charged or dipolar defects in the substrate. As discussed in the Introduction, the wide class of charged or dipolar, localized or extended defects is ubiquitous in ionic oxide as common substrates, so that they represent likely candidates toward the goal of reconciling transmission degradation and substrate defectivity in 2D phases. We study two prototypical cases. First, we focus on the effects of electrostatic defects

on the bulk semiconductor phase. In the second case (to the best of our knowledge, here investigated for the first time) we add a properly tuned electrostatic perturbation at the metal/semiconductor interface, rather than next to a bulk. Our goal in this second case is to find out whether we can use electrostatics to improve, rather than degrade, transmission.

Keeping these two goals in mind, we generate an atomistic model for NbS_2/WSe_2 system A LH with 4 NbS_2 unit and 4 WSe_2 units (see Figure 1a for the original, unperturbed system) was built and subjected to full geometric and lattice relaxation at the DFT level. The chosen system is large enough to enable investigating electrostatic point defects, that we model with few lines of ionic system (LiF) placed symmetrically on both sides of the monolayer (Figure 1b,c) (finally producing a quadrupole perturbation which is compatible with our 3D periodic approach [46]). Note that we place the Li and F atoms at a different height, and that we use double lines of LiF in the middle of the semiconductor region (Figure 1b) or two separate lines of LiF at the interfaces (Figure 1c). The degrees of freedom of our systems are thus the positions of the LiF lines along the transmission direction (z-axis), the distances of the Li atoms from the monolayer, and the differences in height between Li and F atoms. Figures 1d), 1e) and 1f) are the same systems shown in 1a), 1b) and 1c) respectively, repeated in the y-direction, to provide a clearer visualization of the periodicity in the direction orthogonal to transmission.

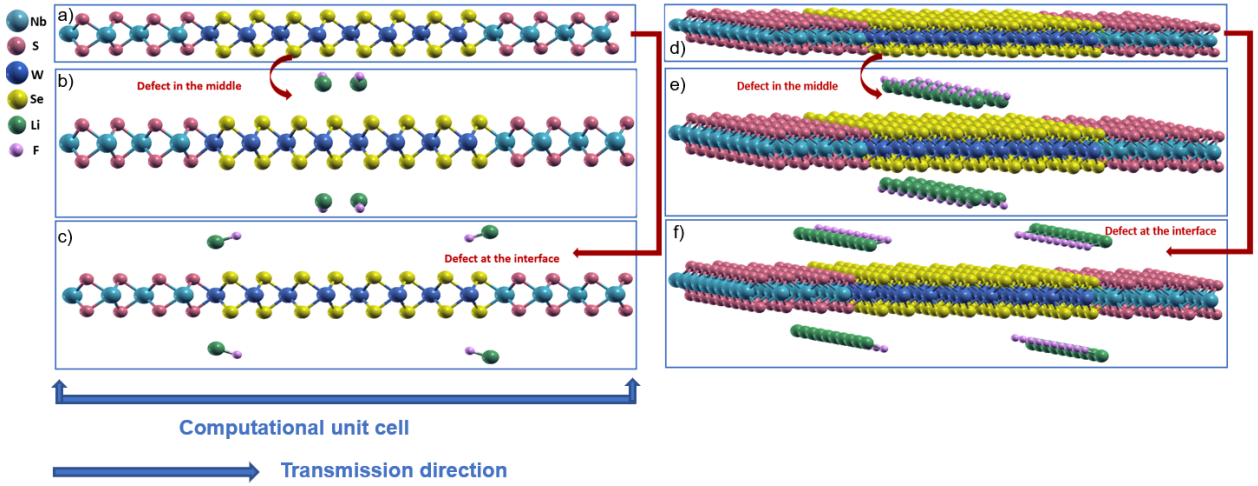

Figure 1. a) NbS_2/WSe_2 monolayer b) Electrostatic defect in the form of LiF in the middle of the semi-conducting phase. c) Electrostatic defect in the form of LiF at the interface. d) unperturbed

system repeated in y-direction e) system with defect in the middle of the semiconducting region repeated in y-direction f) system with defect at the interface repeated in y-direction.

Starting with the first case study, an electrostatic point defect in the substrate, we put two double lines of LiF in correspondence to the middle of the semiconducting region (Figure 1b). The rationale of focusing on the WSe_2 region is because screening effects are weaker in a semiconductor and electrostatic effects on transmission are therefore amplified. After going through many possibilities we select a LiF configuration in which the F atoms is positioned at a height 0.6 Å higher than the Li atom. In general, we note that there is no special reason for the geometric parameters we choose, except that the generated perturbation is at the same time physically reasonable and significant enough to produce observable effects – other choices we have tried produce qualitatively similar results.

In previous work [42], we have shown that on-site electrostatic potential on the site of the nuclei of the atoms is a good descriptor to analyze transmission of 2D systems. Figure S2 shows a 2D plot of the electrostatic potential generated by the bare LiF. To understand its effect on the system, we plot in Figure 2b the electrostatic potential at the site of Nb and W atoms when no monolayer is present (green curve) and compared it with electrostatic potential difference between the perturbed and unperturbed system (red curve) for the case when the defect is in the middle of the semiconducting region. Figure 2d present similar plots for the case in which the defect is located next to the interfaces. From these two curves for both cases we can observe that the electrostatic screening is much stronger in the metallic part of the LH as compared to the semiconducting part, as it could have been expected. Indeed, in Figure 2b) when we compare the green curve with the red curve we can see that the change in the W part is much more prominent than the change in the Nb part. If we look at the electrostatic potential without the monolayer, with only LiF present, and we focus on the Cartesian points where the Nb4, Nb5, W4 and W5 atoms of the monolayer will be positioned, we find that the electrostatic potential generated by LiF produces the following values: -0.139 eV, -0.129 eV, -1.571 eV and -1.571 eV, respectively. Now, when we look at the difference in electrostatic potential on the Nb4, Nb5, W4 and W5 atoms for the unperturbed and the perturbed monolayer, we find that this difference reads: 0.002 eV, 0.002 eV, -0.126 and -0.121 at those sites, respectively. The screening of the LiF electrostatic perturbation at the Nb sites, given by the ratio between the difference in electrostatic potential

and the perturbing "bare LiF" perturbation, is therefore a factor of: 69.5 and 65.5 for Nb4 and Nb5, respectively, and of: 12.5 and 12.9 for W4 and W5 sites, respectively. We can see that the screening in the Nb region is stronger compared to that in the W region.

In previous work [42], we have shown that on-site electrostatic potential on the site of the nuclei of the atoms is a good descriptor to analyze transmission of 2D systems.

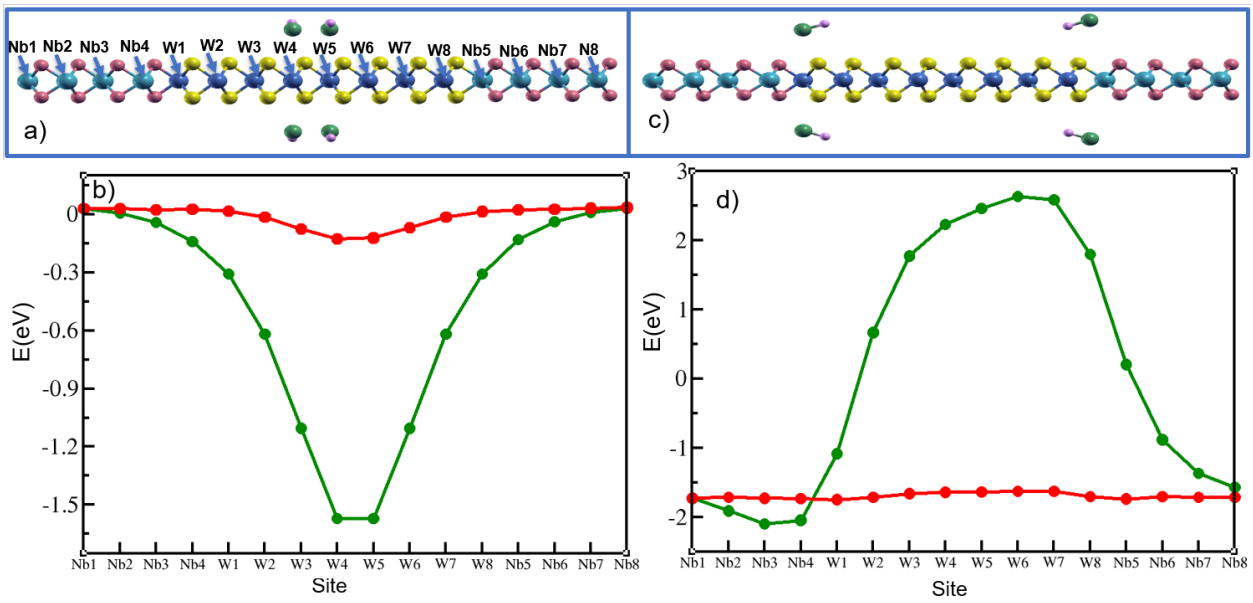

Figure 2: a) System with defect in the middle of the semiconducting region b) Electrostatic potential profile due to defect in the middle of the semiconducting region on Nb and W atomic site without (green) the monolayer. The red curve shows the difference in electrostatic potential between the perturbed and unperturbed system. c) System with defect at the interface d) Same as 2b) but for the defect at the interface.

Now we move on to analyze the effect of the LiF perturbation on the system's transmission. The calculated transmission profile is reported in Figure 3e, where we can appreciate a significant *reduction in transmission in the perturbed system*. To quantitatively rationalize this result, in Figure 3b we report again the electrostatic potential on the W atoms of the unperturbed system shown in Figure 3a and of the perturbed system shown in Figure 3c. As a technical note, to align the two potential profiles with respect to their respective Fermi levels we compare the projected density of states (PDOS) of the W atom at the interface (W1), farthest away from the LiF defect,

finding that the peak of the perturbed (red) system is 0.0128 eV lower in energy than the peak of the unperturbed (purple) system (see Figure 3d). In the unperturbed system the electrostatic potential on the W atoms in the middle are 0.025 eV (W4) and 0.035 eV (W5) below the one at the left interface (W1). In the defected system the W atoms in the middle are 0.167 eV (W4) and 0.172 eV (W5) below the one at the left interface (W1). So there is a decrease of 142(W4)/137(W5) meV of the electrostatic potential for the W atoms in the middle. This happens because we have placed LiF such that the Li atoms on top of the 4^{th} and 5^{th} W atoms are at a vertical distance of 6 Å from the monolayer, whereas the F atoms is positioned at a height 0.6 Å higher than the Li atom. The fact that Li is closer than F to the monolayer brings about a *decrease in the electrostatic potential* in the semiconductor as apparent in Figure 3b. This electrostatic effect may be seen as the analogue of the gate voltage that is introduced in FET devices to modulate transmission (note that if we switch the heights of the Li and F atoms, which is tantamount to inverting the polarity of the electrostatic defect i.e., of the gate, we see an increase in the electrostatic potential and an increase in transmission as consistent with the proposed reasoning). Following a procedure proposed in Ref.[42], we further elaborate these results by plotting in Figures 3f),g) the density of states (DOS) of the WSe_2 fragment along the transmission direction with their centers shifted (aligned) according to the atomic electrostatic potential profiles of Figure 3b). The WSe_2 fragment representing the WSe_2 bulk is shown in Figure S10 b), and its DOS in Figure S10 c), where the change in DOS is presented with a gradient of color and the values associated with the color graduation are indicated in the bar. Here we can clearly see that, as a consequence of lowering the electrostatic potential in the middle of WSe_2, there are less states available for transport in the perturbed with respect to the unperturbed system, as highlighted by the circled area in Figure 3g). This quantitatively rationalizes the observed transmission profiles. Indeed, it can be seen that the maximum in transmission is decreased from 0.16 in the unperturbed system to 0.06 in the perturbed system as an effect of a misalignment of around 140 meV in the electrostatic potential. To verify our findings, we also looked at the LDOS of atoms in the semiconducting region, of the heterostructure. The results are presented in SM Figure S11, It shows that it is indeed a decrease/increase in the DOS of the W atoms which determines the decrease/increase of the transmission.

Note in passing that we find a finite value of the DOS at the Fermi energy within the WSe_2 region because of a charge transfer at the interface locally shifting the valence band of WSe_2 [42]. This shift should in principle decay to zero away from the interface but in this case it remains finite due to the small size of the DFT model system.

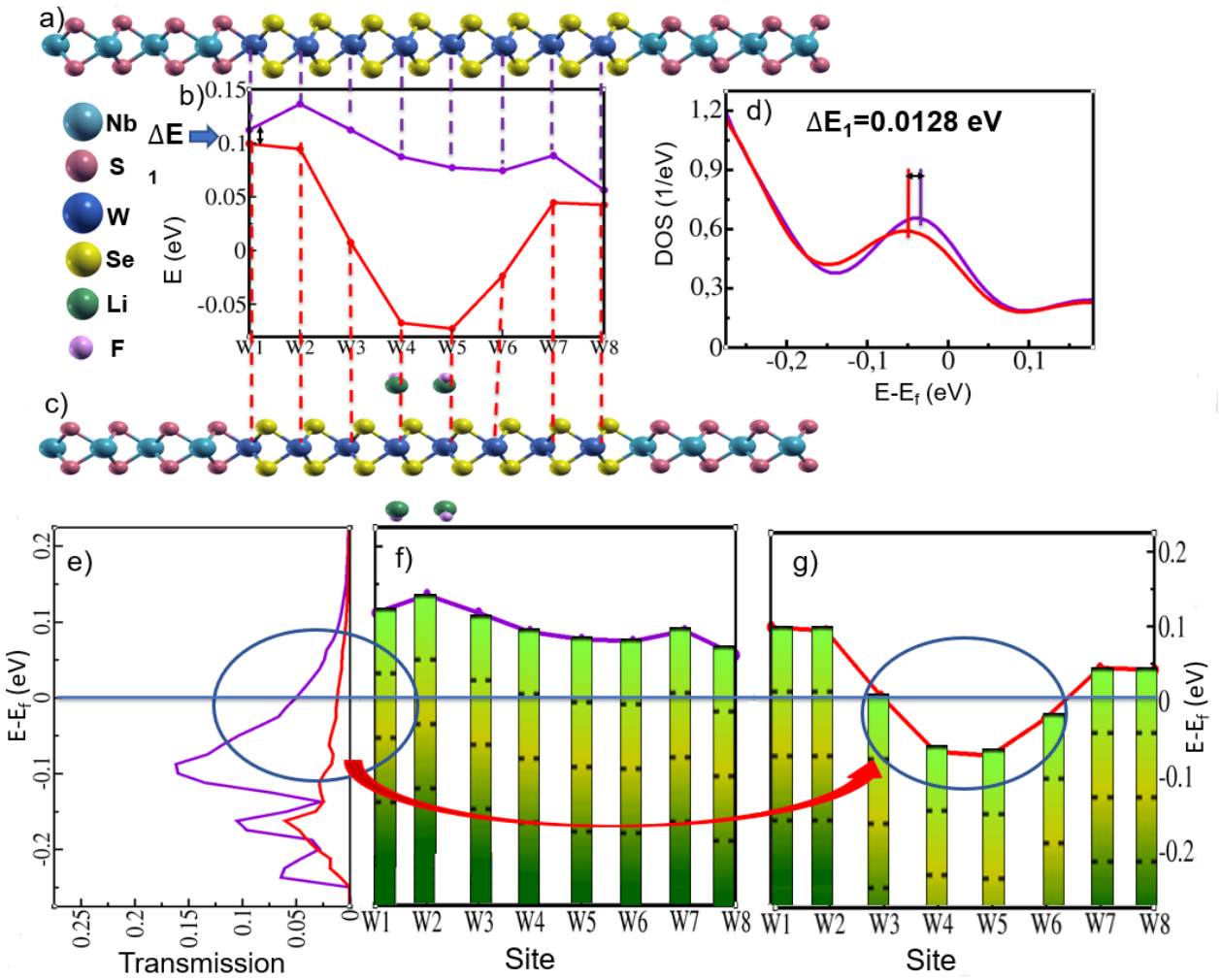

Figure 3. a) Side view of the NbS_2-WSe_2 monolayer without any perturbation b) Electrostatic potential profiles on the sites of W atoms for the unperturbed (purple) and perturbed (red) system. c) Side view of the NbS_2-WSe_2 monolayer with perturbation in the middle of the semiconducting region d) PDOS of W atom at the interface of the unperturbed (purple) and perturbed (red) systems. e) Transmission profile of the unperturbed (purple) and perturbed (red) systems. Electrostatic potential alignment of the unperturbed system in f) and perturbed system in g) showing the states available for electron transmission using the color bar from the DOS of

the fragment shown in SI (Fig S10), with the circled area showing the reduction in DOS and its effect on transmission.

A natural question arising at this point is whether this effect is seen experimentally. To check this, we look at experimental work in which the effect of substrate has been studied. T. Jin et al [47] investigated and compared the electrical properties of single-layer MoS_2 devices both supported on a substrate and freely suspended, and found that the electrical performance was influenced significantly by the substrate, with the suspended devices exhibiting 2-10 times improved mobility and on/off ratio. In Ref.[30], a MoS_2 monolayer was grown and transferred over a SiO_2/Si substrate with holes. The photoluminescence (PL) intensity of the suspended MoS_2 region over the hole was found to be much brighter than that of the MoS_2 region over the substrate. The effect of a large variety of substrates on the PL intensity has also been studied in Ref.[48]. Schneider et al. [49] have shown that the PL spectra of thin film of MoS_2 on Si/SiO_2 substrate is quenched compared to the one on sapphire substrate dure to substrate-induced interference. D. Liu, at. al. [56] studied the effect of substrate on the photoluminescence of monolayer of WSe_2. They concluded that the PL intensities changes drastically for different substrates such as sapphire, SiO_2/Si, quartz .

S. Lippert at. al. [57] also studied the effect of different substrate on the optical properties of monolayer WSe_2, showing that the Pl spectra varies for different substrate. Freestanding WSe_2 was also studied by N. Mondal et.al [27], who compared photoluminescence spectra of suspended WSe_2 with that of WSe_2 grown on fused silica substrate. They found an enhanced intensity of the PL spectra when WSe_2 was free-standing. Qualitatively, the findings in this study are homologous to the previous studies on MoS_2, supporting the idea that the physics we are trying to understand is general and applies to all similar TMDCs.

These results suggest that our electrostatic hypothesis is worth deepening. Indeed, a perusal of the literature suggests that a correlation between better growth protocols producing to less defects in the substrate and a better quality of transmission in the TMD systems can indeed be found. This should trigger further and more detailed experimental investigations.

Once shown that electrostatic defects can reduce conductance, we asked ourselves the question whether it is possible to use such effect in the opposite direction, i.e., to increase conductance. To give an answer to this, we took a closer look at the unperturbed system and try to understand

from the electrostatic-potential analysis which modifications could be introduced to improve transmission. Note first that our LH model is constructed as a metal/semiconductor/metal system, so that we have two NbS_2/WSe_2 interfaces: a left and a right one. This arrangement replicates the typical situation in FET devices where two metal electrodes bracket a semiconductor producing a metal/semiconductor and a semiconductor/metal junction. A specific feature of the present case is that these two interfaces are non-symmetric due to geometric reasons of incompatibility between hexagonal pattern and mirror-plane symmetry (see Ref.[42] for a more detailed discussion). This is the reason why the electrostatic potential profile in Figures 3b) and 4b) is non-symmetric. the electrostatic potential at the right end (W8) is 0.056 eV lower than the electrostatic potential at the left interface (W1). This misalignment can however decrease transmission. To find the optimum position of LiF line over the heterostructure, we placed LiF at different positions and heights above the heterostructure. By analyzing the transmission in these cases, we have identified the factors affecting transmission. Asymmetry of the potential is one of the recognizable descriptors which affects the transmission profile, which is reasonable because the hybridization between electronic states is maximized when their energies are degenerate, whereas a difference in energy will decrease hybridization and consequently transmission. Another recognizable descriptor was the flatness of the potential. We therefore played with these two factors to create the configuration of Fig. 1c,f. We can thus argue that “curing” (decreasing) the asymmetry of the potential and increasing the flatness of the electrostatic potential should increase conductance. To have W1 and W8 at the same level we need to destabilize the right side and/or stabilize the left side. To achieve this, we tried out several configurations. In these configurations we explored the two degrees of freedom at hand, i.e., the height of LiF from the monolayer as well as the relative height difference between the Li and F. We finally arrived at a configuration in which we placed two lines of LiF, one at each interface. At the right interface, LiF is placed such that F atom is on top of the W atom at a height of 6 A. At the left interface we placed Li on top of W and at a slightly reduced height of 5.7 A (Figure 4a). We can qualitatively understand the effect of these lines of LiF at the two interfaces by looking at the potential profile without the LH in Figure 2d, where we see that the added bare LiF perturbation produces an electrostatic potential at the right interface significantly higher (2.84 eV) than at the left interface. Now, looking at Figure 4b), where we report the potential profiles of both the unperturbed (purple) and perturbed (red) systems aligned according to the PDOS of their

respective W1 atoms given in Figure 4d), one can see that the potential alignment is much improved, and the electrostatic potential on the right interface (W8) is now only 0.014 eV lower than the potential on the W atom at the left interface (W1). An increase in the potential on the W atoms in the middle of WSe_2 is also observed resulting in a smoother potential profile in the middle of the system. In Figure 4e) we report the transmission profiles for the unperturbed system (purple curve) and for the perturbed system (red curve). We find a clear *increase in transmission* as a result of the electrostatic perturbation, with the maximum in the transmission profile increasing from 0.16 to 0.24.

This results can be further rationalized via a DOS alignment analysis similar to the one conducted for the first study case. This analysis is shown in in Figure 4f)-4g), where the circled area in the perturbed system highlight that we now have more states available for transmission, whence the higher conductance. Further, looking at Figure S10 one can identify a range of ~0.08 eV around the peak in DOS (at 0.2 eV) as the states responsible for the maximum transmission. Now, when we look at Figure 4f and look at DOS around the transmission peak in a range of ~0.08 eV (indicated by dots separating the bars into section of width 0.08 eV each) and follow it along the potential profiles in both the systems, we find that in this range only 0.04 eV of the perturbed system transmission peak is included. This indicates a shift in the peak in the transmission when we go from unperturbed to perturbed system. We can thus conclude that, by putting an electrostatic perturbation on one interface different than the one at the other interface in order to re-align the electrostatic potential at the boundaries and simultaneously to make the electrostatic potential profile flatter, we can achieve a significant increase in transmission.

Before concluding, we note that the present work is intended as a proof-of-principle study. Limitations in computational resources and technical constraints such as those ensuing from 3D periodicity of the QE code (see the SI), force us to consider model systems, both in terms of size and in terms of electrostatic perturbations we are able to introduce. Nevertheless, we believe that the two study cases here reported correspond to the two general classes of electrostatic effects on transport in 2D materials.

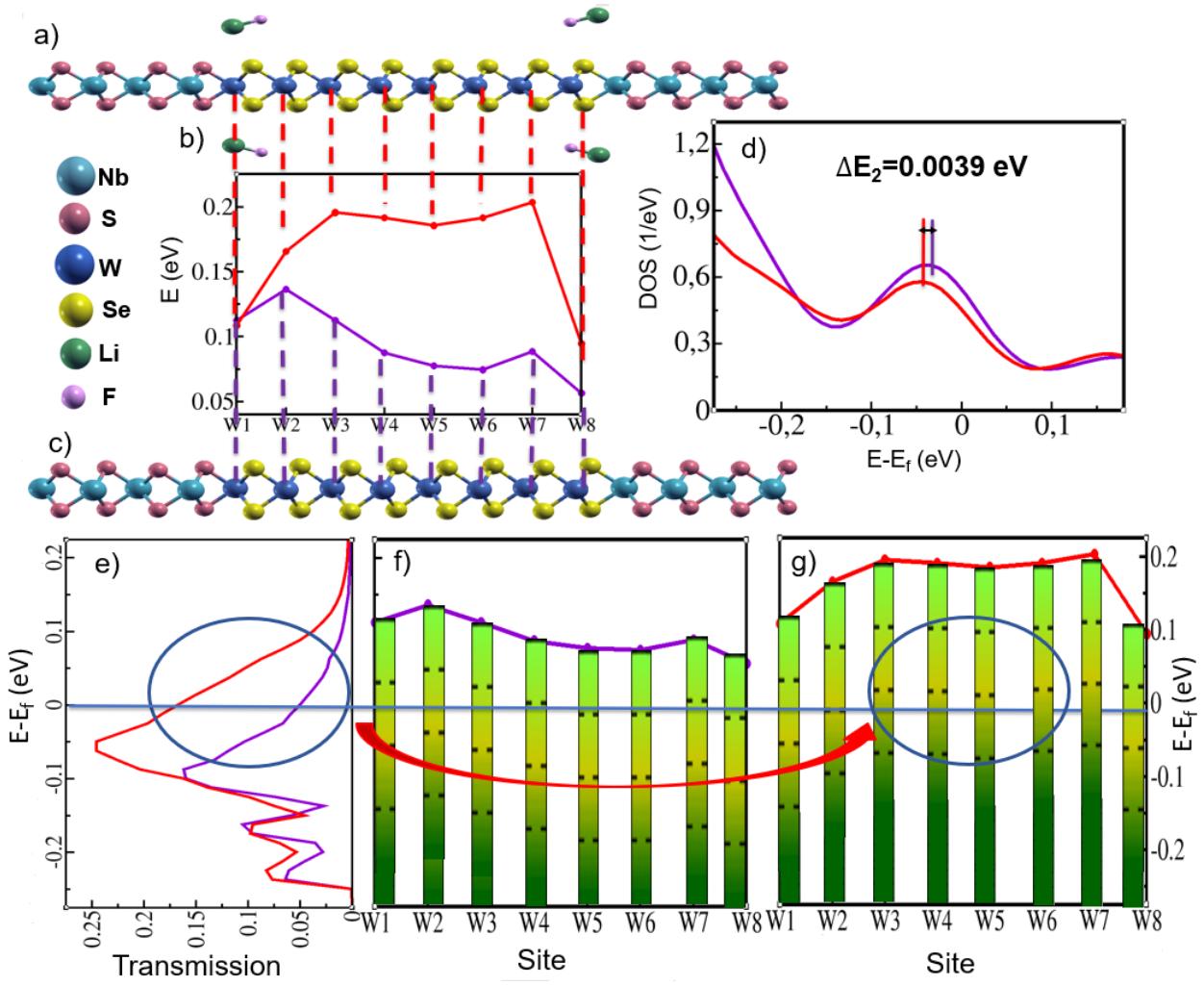

Figure 4. a) Side view of the NbS_2-WSe_2 monolayer with perturbation at the interface; b) Electrostatic potential profiles on the sites of W atoms for the unperturbed (purple) and perturbed (red) system; c) Side view of the NbS_2-WSe_2 monolayer without any perturbation; d) PDOS of W atom at the interface of the unperturbed (purple) and perturbed (red) systems. e) Transmission profile of the unperturbed (purple) and perturbed (red) systems. Electrostatic potential alignment of the unperturbed system in f) and perturbed system in g) showing the states available for electron transmission using the color bar from the DOS of the fragment in Figure S10.

4. Conclusions

In summary, here we studied the effect of electrostatic perturbations on the transmission of 2D LHs, taking a monolayer NbS_2/WSe_2 system as a prototypical example of a metal/semiconductor junction. We introduce electrostatic point defects in the form of LiF lines in two different

configurations/cases, aimed at modelling two different physical phenomena, and use the electrostatic potential profile as the descriptor determining transmission. In a former case, we place the defect in the middle of the semiconducting region, with the goal of mimicking an electrostatic (charged or dipolar) defect in the substrate. This defect configuration stabilizes the electrostatic potential in the middle of the semiconducting region, analogously to a gate effect. Using an electrostatic potential and DOS analysis [42], we find that this makes that there are less available states for transmission in that region, leading to a significant reduction in transmission (potentially rationalizing experimental observations). In a latter case, we exploit the asymmetry of the system's interfaces to our benefit and perturb them differently to reduce their asymmetry, simultaneously flattening the electrostatic potential profile, and demonstrate how this leads to an increase in the transmission, thus providing us with a tool at our disposal to enhance transmission in such systems.

Acknowledgements

The authors thank the QUEFORMAL project for the financial support. The QUEFORMAL project has received funding from the European Union's Horizon 2020 Research and Innovation Program under the Marie Skłodowska-Curie grant agreement no. 829035. We thank the ISCRA programme at the Cineca supercomputer center (Bologna, Italy) for providing computational resources.

Supplemental Material

Molecular dynamics of the LH to test its thermodynamic stability. Details of calculations, including plots of 2D electrostatic potential profiles. Details of the transmission calculations. Details of the Wannier calculations with figures of band structures obtained using DFT and Wannier for both unperturbed and perturbed systems. Density of state of the unit cell from the semiconducting region. Density of states of all W and Se atoms from the semiconducting region.

References

[1]: Y. Wu, Y-m. Lin, A. A. Bol, K. A. Jenkins, F. Xia, D. B. Farmer, Y. Zhu, P. Avouris,. Nature., **472**, 74-78, (2011).

[2]: Y.-M. Lin, K. A. Jenkins, A. Valdes-Garcia, J. P. Small, D. B. Farmer, P. Avouris,. Nano Lett.**, 9**, 422-426, (2009).

[3]: B. Radisavljevic, A. Kis, Nat. Mater., **12**, 815-820, (2013).

[4]: J. N. Coleman, M. Lotya, A. O'Neill, S. D. Bergin, P. J. King, U. Khan, K. Young, A. Gaucher, S. De, R. J. Smith, I. V. Shvets, S. K. Arora, G. Stanton, H.-Y. Kim, K. Lee, G. T. Kim, G. S. Duesberg, T. Hallam, J. J. Boland, J. J. Wang, J. F. Donegan, J. C. Grunlan, G. Moriarty, A. Shmeliov, R. J. Nicholls, J. M. Perkins, E. M. Grieveson, K. Theuwissen, D. W. McComb, P. D. Nellist, V. Nicolosi, Science, **331**, 568-571 (2011).

[5]: Q. H. Wang, K. Kalantar-Zadeh, A. Kis, J. N. Coleman, M. S. Strano, Nat. Nanotechnol., **7**, 699-712, (2012).

[6]: Xi, X.; Berger, H.; Forró, L.; Shan, J.; Mak, K. F. Gate Tuning of Electronic Phase Transitions in Two-Dimensional $NbSe_2$. Phys. Rev. Lett., **117**, 106801 (2016).

[7]: G. Eda, H. Yamaguchi, D. Voiry, T. Fujita, M. Chen, M. Chhowalla, Nano Lett.**, 11**, 5111-5116 (2011).

[8]: K. Lee, H.-Y. Kim, M. Lotya, J. N. Coleman, G.-T. Kim, G. S. Duesberg, Adv. Mater., **23,** 0935-9648 (2011).

[9]: J. D. Cain, F. Shi, J. Wu, V. P. Dravid, ACS Nano, **10**, 5440-5445, (2016).

[10]: X. Duan, C. Wang, J. C. Shaw, R. Cheng, Y. Chen, H. Li, X. Wu, Y. Tang, Q. Zhang, A. Pan, J. Jiang, R. Yu, Y. Huang, X. Duan, Nat. Nanotechnol., **9**, 1024-1030, (2014).

[11]: C. Huang, S. Wu, A. M. Sanchez, J. J. P. Peters, R. Beanland, J. S. Ross, P. Rivera, W. Yao, D. H. Cobden, X. Xu, Nat. Mater., **13**, 1096-1101 (2014).

[12]: X. Hong, J. Kim, S.-F. Shi, Y. Zhang, C. Jin, Y. Sun, S. Tongay, J. Wu, Y. Zhang, F. Wang, Nat. Nanotechnol., **9**, 682-686, (2014).

[13]: Y. Liu, J. Guo, E. Zhu, L. Liao, S. J. Lee, M. Ding, I. Shakir, V. Gambin, Y. Huang, X. Duan, Nature, **557**, 696-700, (2018).

[14]: C. M. Went, J. Wong, P. R. Jahelka, M. Kelzenberg, S. Biswas, M. S. Hunt, A. Carbone, H. A. Atwater, Sci. Adv., **5**, eaax6061, (2019).

[15]: G. Iannaccone, F. Bonaccorso, L. Colombo, G. Fiori, Nat. Nanotechnol., **13**, 183-191, (2018).

[16]: Y. Zhou, G. Scuri, J. Sung, R. J. Gelly, D. S. Wild, K. De Greve, A. Y. Joe, T. Taniguchi, K. Watanabe, P. Kim, M. D. Lukin, H. Park, Phys. Rev. Lett.**, 124**, 027401, (2020).

[17]: Y. Gong, J. Lin, X. Wang, G. Shi, S. Lei, Z. Lin, X. Zou, G. Ye, R. Vajtai, B. I. Yakobson, H. Terrones, M. Terrones, B. K. Tay, J. Lou, S. T. Pantelides, Z. Liu, W. Zhou, P. M. Ajayan, Nat. Mater., **13**, 1135-1142, (2014).

[18]: M. Y. Li, Y. Shi, C. C. Cheng, L. S. Lu, Y. C. Lin, H. L. Tang, M. L. Tsai, C. W. Chu, K. H. Wei, Jr-H. He, W. H. Chang, K. Suenaga, L. J. Li, Science, **349**, 524-528, (2015).

[19]: C. Zhang, Y. Chen, J. K. Huang, X. Wu, L. J. Li, W. Yao, J. Tersoff, C. K. Shih, Nat. Commun., **7**, 10349, (2016).

[20]: H. G. Shin, H. S. Yoon, J. S. Kim, M. Kim, J. Y. Lim, S. Yu, J. H. Park, Y. Yi, T. Kim, S. C. Jun, S. Im, Nano Lett., **18**, 1937-1945, (2018).

[21]: Y. An, M. Zhang, D. Wu, Z. Fuac, K. Wang, J. Mater. Chem. C, **4**, 10962-10966, (2016).

[22]: C. Mu, W. Wei, J. Li, B. Huang, Y. Dai, Mater. Res. Express., **5**, 046307, (2018).

[23]: Y. An, M. Zhang, D. Wu, Z. Fu, K. Wang, J. Mater. Chem. C., **4**, 10962-10966, (2016).

[24]: Y. N. Wen, M. G. Xia, S. L. Zhang, Appl. Surf. Sci., **371**, 2354-2360, (2016).

[25]: W. Wei, Y. Dai, B. Huang, Phys. Chem. Chem. Phys.,**18**, 15632-15638, (2016).

[26]: N. Scheuschner, O. Ochedowski, A. M. Kaulitz, R. Gillen, M. Schleberger, J. Maultzsch,. Phys. Rev. B., **89**, 125406, (2014).

[27]: N. Mondal, N. Azam, Y. N. Gartstein, M. M- Samani and A. V. Malko, Adv. Mater. **34,** 2110568 (2022).

[28]: S. Y. Zhou, G.-H. Gweoni, A. V. Fedorov, P. N. First, W. A. De Heer, D.-H. Lee, F. Guinea, A. H. C. Neto, A. Lanzara, Nat. Mater., **6**, 770-775, (2007).

[29]: K. F. Mak, C. Lee, J. Hone, J. Shan, T. F. Heinz,. Phys. Rev. Lett, **105**, 136805, (2010).

[30]: K. Liu, Q. Yan, M. Chen, W. Fan, Y. Sun, J. Suh, D. Fu, S. Lee, J. Zhou, S. Tongay, J. Ji, J. B. Neaton, J. Wu,. Nano Lett.**, 14,** 5097-5103, (2014).

[31]: Y. Sun, R. Wang, K. Liu,. Applied Physics Reviews, **4**, 011301, (2017).

[32]: S. Kataria, S. Wagner, T. Cusati, A. Fortunelli, G. Iannaccone, H. Pandey, G. Fiori, M. C. Lemme, Adv. Mater. Interfaces, **4**, 1700031, (2017).

[33]: L. Ma, Y. Tan, M. Ghorbani-Asl, R. Boettger, S. Kretschmer, S. Zhou, Z. Huang, A. V. Krasheninnikov, F. Chen. Nanoscale, **9**, 11027, (2017).

[34]: S. Zhang, C.-G. Wang, M.-Y. Li, D. Huang, L.-J. Li, W. Ji, S. Wu, Phys. Rev. Lett., **119**, 046101, (2017).

[35]: X. Ma, Y.-Y. Liu, L. Zeng, J. Chen, R. Wang, L.-W. Wang, Y. Wu, X. Jiang,. ACS Appl. Mater. Interfaces, **14**, 2185-2193, (2022).

[36]: P. Rinke, A. Schleife, E. Kioupakis, A. Janotti, C. Ro¨dl, F. Bechstedt, M. Scheffler, and C. G. Van de Walle, Phys. Rev. Lett., 108, 126404 (2012).

[37]: M. G. Sensoy, D. Vinichenko, W. Chen, C. M. Friend, and E. Kaxiras, Phys. Rev. B **95**, 014106 (2017).

[38]: X. Wang, J. Wu, Y. Zhang, Y. Sun, K. Ma, Y. Xie, W. Zheng, Z. Tian, Z. Kang, Y. Zhang, Adv. Mater. , 2206576, (2023).

[39]: Y. Guo, X. Wei, J. Shu, B. Liu, J. Yin, C. Guan, Y. Han, S. Gao, and Q. Chen, Appl. Phys. Lett. **106**, 103109 (2015).

[40]: C-.H. Chang, X. Fan, S-. H. Lin, and Jer-Lai Kuo, Phys. Rev. B., **88,** 195420, (2013).

[41]: Z. Wang, M. Tripathi, Z. Golsanamlou, P. Kumari, G. Lovarelli, F. Mazziotti, D. Logoteta, G. Fiori, L. Sementa, G. M. Marega, H. G. Ji, Y. Zhao, A. Radenovic, G. Iannaccone, A. Fortunelli, and A. Kis, Adv. Mater., **35,** 2209371, (2023).

[42]: Z. Golsanamlou, L. Sementa, T. Cusati, G. Iannaccone, A. Fortunelli,. Adv. Theory Simul., **4**, 2100164, (2021).

[43]: Z. Golsanamlou, P. Kumari, L. Sementa, T. Cusati, G. Iannaccone, A. Fortunelli,. Adv. Electron. Mater, **8**, 2200020, (2022).

[44]: Q. Liang, Q. Zhang, X. Zhao, M. Liu, and A. T. S. Wee, ACS Nano, **15,** 2165-2181, (2021).

[45]: S. Wang, G-. D. Lee, S. Lee, E. Yoon and J. H. Warner, ACS Nano, **10,** 5419-5430, (2016).

[46]: V. R. Saunders, C. Freyria-Fava, R. Dovesi, L. Salasco, C. Roetti, Molecular Physics, **77**, 629-665, (1992).

[47]: T. Jin, J. Kang, E. S. Kim, S. Lee, C. Lee, Journal of Applied Physics, **114**, 164509, (2013).

[48]: M. Buscema, G. A. Steele, H. S. J. Van der Zant, A. C.- Gomez, Nano Res., **7**, 561-571, (2014).

[49]: D. S. Schneider, A. Grundmann, A. Bablich, V. Passi, S. Kataria, H. Kalisch, M. Heuken, A. Vescan, D. Neumaier, M. C. Lemme, ACS Photonics, **7**, 1388-1395, (2020).

[50]: P. Giannozzi, S. Baroni, N. Bonini, M. Calandra, R. Car, C. Cavazzoni, D. Ceresoli, G. L. Chiarotti, M. Cococcioni, I. Dabo, A. D. Corso, S. de Gironcoli, S. Fabris, G. Fratesi, R. Gebauer, U. Gerstmann, C. Gougoussis, A. Kokalj, M. Lazzeri, L. Martin-Samos, N. Marzari, F. Mauri, R. Mazzarello, S. Paolini, A. Pasquarello, L. Paulatto, C. Sbraccia, S. Scandolo, G. Sclauzero, A. P. Seitsonen, A. Smogunov, P. Umari, R. M. Wentzcovitch,. J. Phys.: Condens. Matter, **21**, 395502, (2009).

[51]: P. Giannozzi, O. Andreussi, T. Brumme, O. Bunau, M. B. Nardelli, M. Calandra, R. Car, C. Cavazzoni, D. Ceresoli, M. Cococcioni, N. Colonna, I. Carnimeo, A. D. Corso, S. de Gironcoli, P. Delugas, R. A. DiStasio, A. Ferretti, A. Floris, G. Fratesi, G. Fugallo, R. Gebauer, U. Gerstmann, F. Giustino, T. Gorni, J. Jia, M. Kawamura, H.-Y. Ko, A. Kokalj, E. Küçükbenli, M. Lazzeri, M. Marsili, N. Marzari, F. Mauri, N. L. Nguyen, H.-V. Nguyen, A. Otero-de-la-Roza, L. Paulatto, S. Poncé, D. Rocca, R. Sabatini, B. Santra, M. Schlipf, A. P. Seitsonen, A. Smogunov,

I. Timrov, T. Thonhauser, P. Umari, N. Vast, X. Wu, S. Baroni,. J. Phys.: Condens. Matter, **29**, 465901, (2017).

[52]: J. Perdew, K. Burke, M. Ernzerhof,. Phys. Rev. Lett., **77**, 3865, (1996).

[53] N. Marzari, D. Vanderbilt,. Phys. Rev. B., **56**, 12847, (1997).

[54]: A. A. Mostofi, J. R. Yates, Y. S. Lee, I. Souza, D. Vanderbilt, N. Marzari,. Comput. Phys. Commun, **178**, 685-699, (2008).

[55]: Computational 2D materials database, https://cmrdb.fysik.dtu.dk/ c2db/

[56]: D. Liu, X. -Q. Yan, H. -W. Guo, Z. -B. Liu, W. -Y. Zhou, and J. -G. Tian, Journal of Applied Physics **128**, 043101 (2020).

[57]: S. Lippert, L. M. Schneider, D. Renaud, K. N. Kang, O. Ajayi, J. Kuhnert, M. -U. Halbich, O. M Abdulmunem, X. Lin and K. Hassoon, 2D Mater. **4**, 025045, (2017).

Supplemental Material for:

Electrostatic tuning of transmission in NbS_2/WSe_2 2D Lateral Hetero-Structures: A computational study

Poonam Kumari[1], Zahra Golsanamlou[1], Alexander Smogunov[2], Luca Sementa[1,*], Alessandro Fortunelli[1,*]

[1] CNR-ICCOM and IPCF, Consiglio Nazionale delle Ricerche, via G. Moruzzi 1, Pisa 56124, Italy

[2] SPEC, CEA, CNRS, Université Paris-Saclay, CEA Saclay, Gif-sur-Yvette Cedex, 91191 France

1. The Computational Model

1.1.NbS_2/WSe_2 Monolayer

The thermodynamic stability of the monolayer heterostructure was tested using molecular dynamics (MD) simulation. The MD simulation was performed at 300 K temperature with a time step of 5x10-^{4} psec for 3 osec (6000 steps). Figure S1 shows the structure at the end of 6000 steps, energy and temperature fluctuations for the last 4000 steps. The energy fluctuations are less than 0.5 eV and the temperature dispersion is 50 on an average. The system remains intact as well.

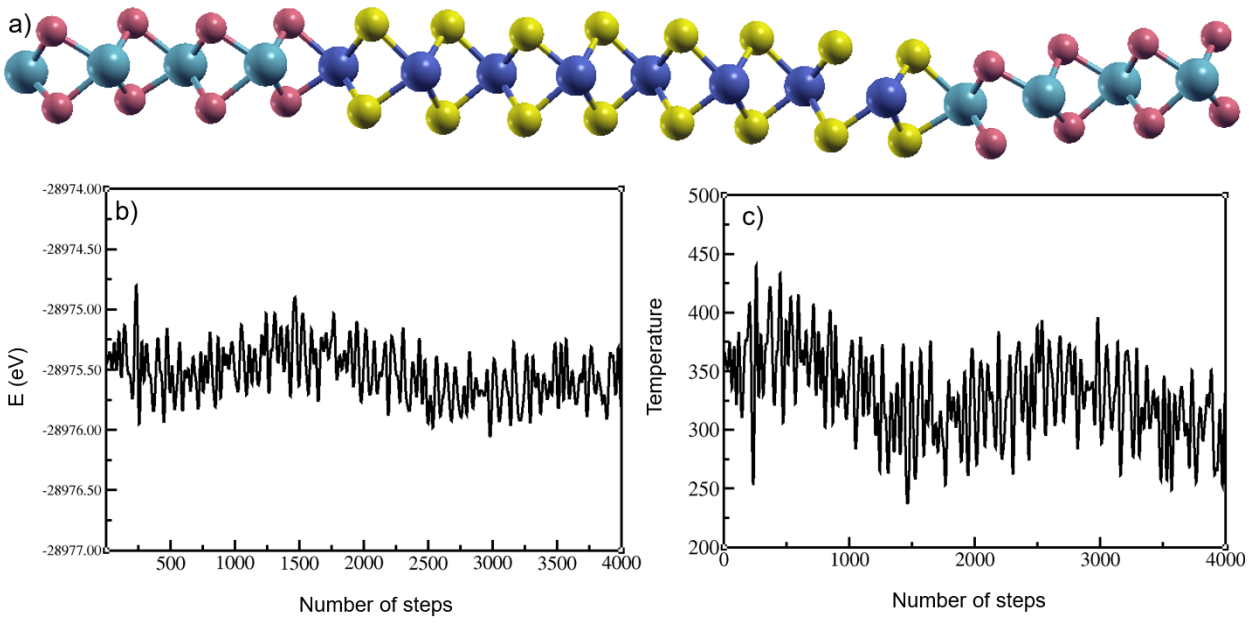

Figure S1 a) structure at the end of 6000 steps, b) fluctuation in energy of the system and c) fluctuation in temperature for the last 4000 steps of MD simulation.

1.2 Defect

LiF, being an ionic compound, is a good model of an electrostatic perturbation. A charge density analysis tells us that LiF essentially corresponds to a charge of +0.4 and -0.4 atomic units on the Li cations and F anions, respectively. Note that we do not relax the system after introducing the electrostatic perturbation to avoid mixture of geometric effects into our analysis. Note also that the use of three-dimensional (3D) periodic modeling within the QE code allows us to reduce the number of atoms in the unit cell and thus achieve a feasible computational effort, with the drawback that periodic conditions also introduce constraints in the physical model as the unit cell can only have a quadrupole in 3D (not a charge, not a dipole) to avoid electrostatic divergence [1].

2. Details of the calculations

2.1 Electrostatic Potential

We recall that the electrostatic potential we plot is the self-consistent background in which the electron moves and forms the main component of the Kohn-Sham potential. With respect to the Kohn-Sham potential, our electrostatic potential only lacks the exchange correlation term, which we prefer not to include since it is more sensitive to numerical errors.

Figure S2 and S3 shows the affect of the two defect configurations used.

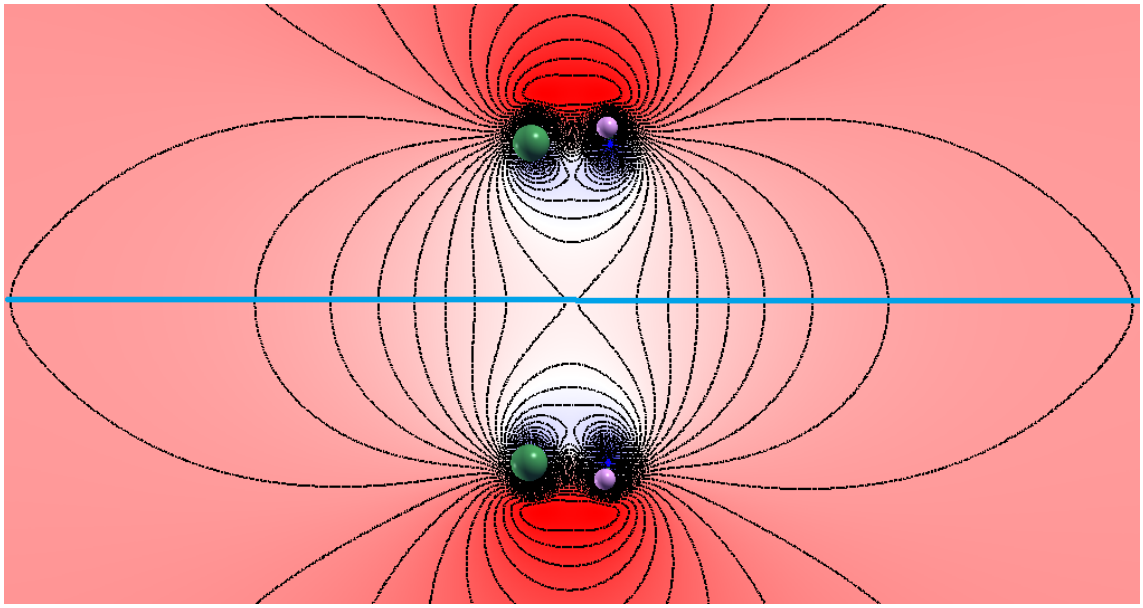

Figure S2: 2D plot of the electrostatic potential generated by the bare LiF perturbation, when the middle of the semiconductor region was perturbed. Blue line represents the position of the monolayer.

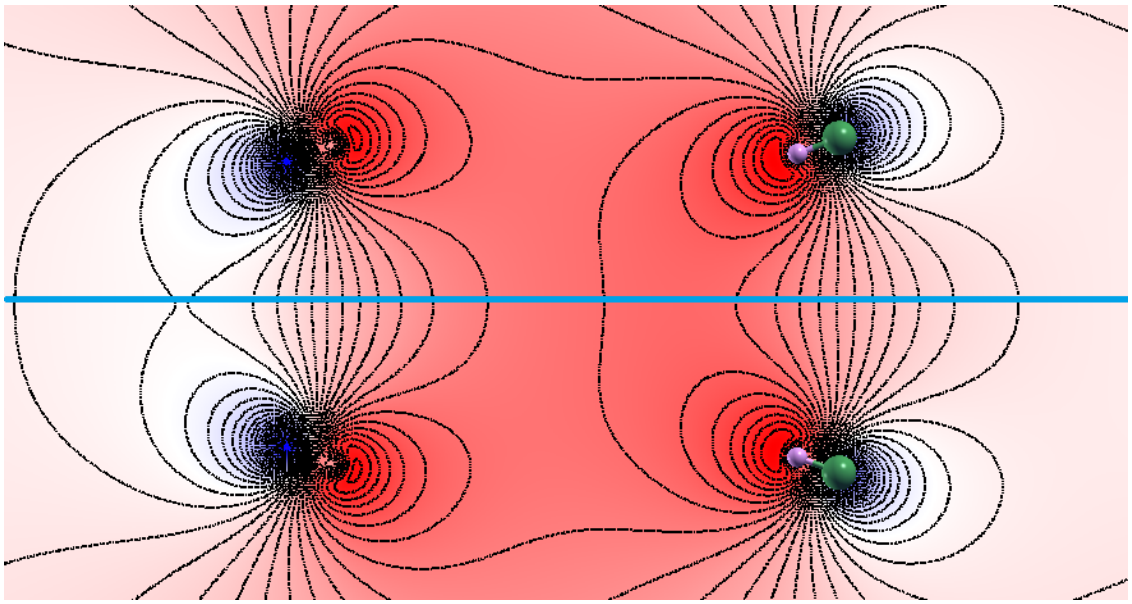

Figure S3: 2D plot of the electrostatic potential generated by the bare LiF perturbation, when the interface was perturbed. Blue line represents the position of the monolayer.

Figure S4 shows the electrostatic potential at the site of Nb atoms in the unperturbed system (purple) and the system where the middle of the semiconducting region has been perturbed (red). Compared to the semiconducting part we can see that here the change in electrostatic potential is much smaller. The alignment of the unperturbed systems has been achieved with the method given in Ref.[2] and the alignment of the perturbed systems has been achieved in a similar manner as the semiconducting part where the PDOS of Nb1 atom has been taken as reference and the difference in the peak of the PDOS has been used to align both the curves with respect to each other.

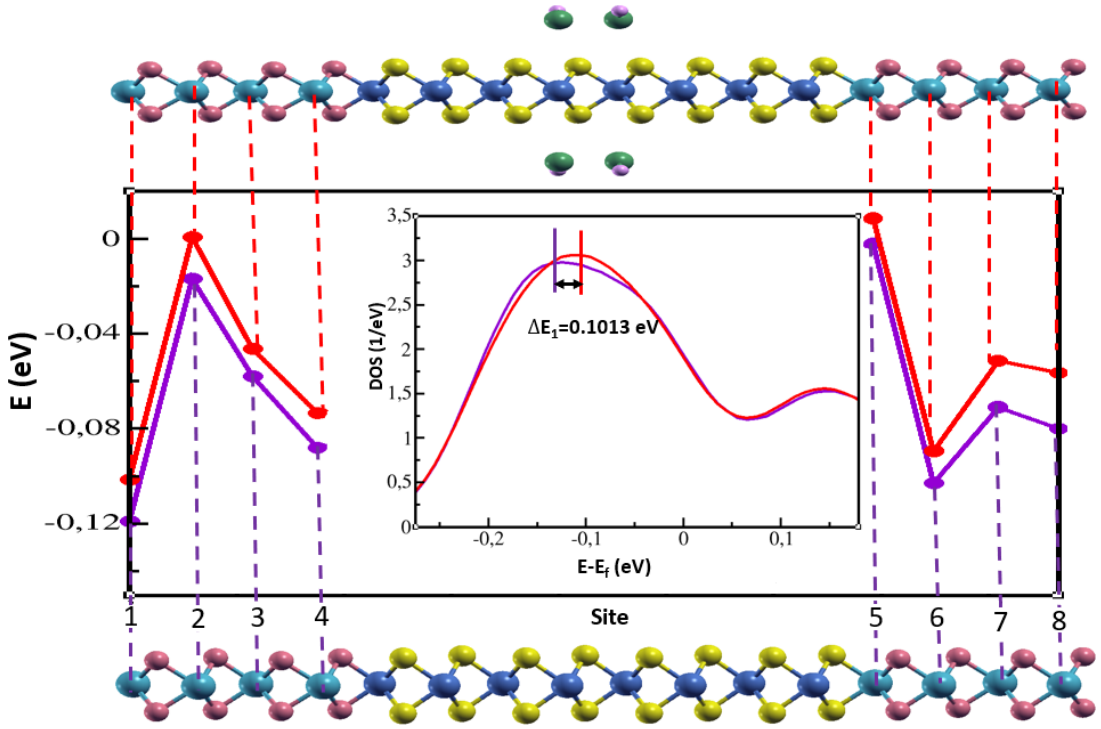

Figure S4: electrostatic potential on the site of Nb atoms for the unperturbed system (purple) and the system where the middle of semiconducting region is perturbed. Inset shows the PDOS of Nb1 for both the systems.

Figure S5 shows the electrostatic potential at the site of Nb atoms in the unperturbed system (purple) and the system where the interfaces have been perturbed (red).

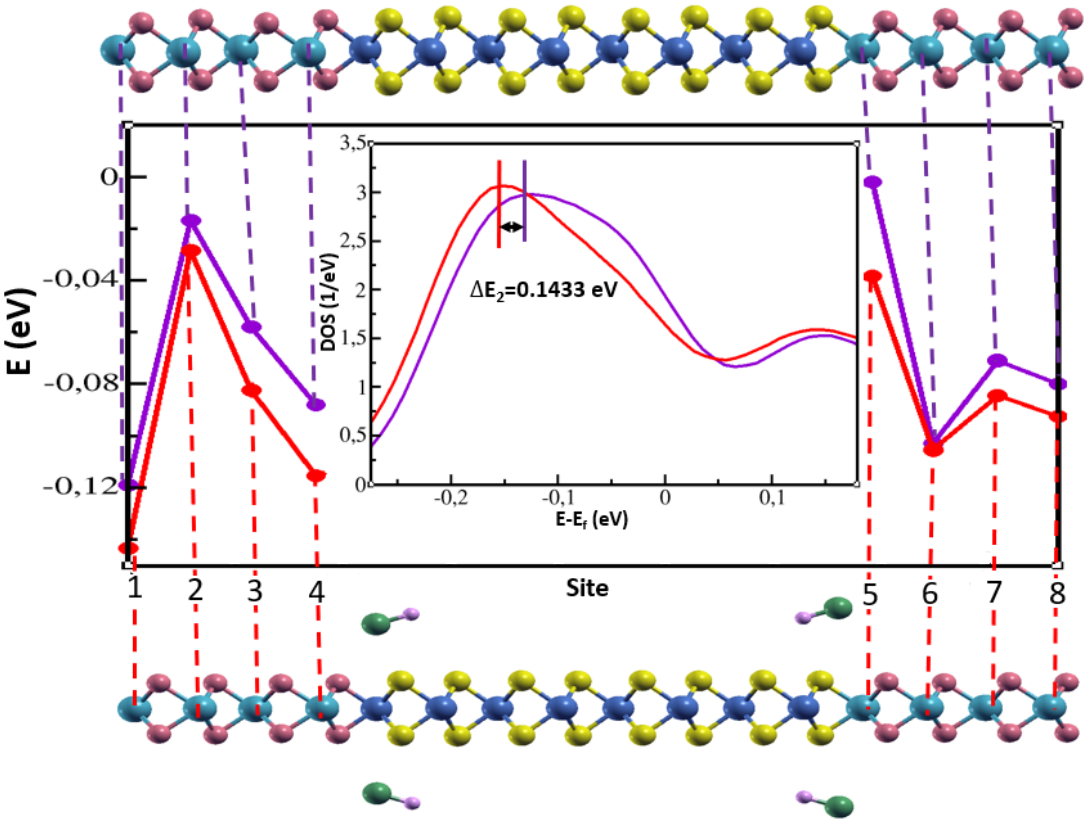

Figure S5: electrostatic potential on the site of Nb atoms for the unperturbed system (purple) and the system where the interfaces have been perturbed. Inset shows the PDOS of Nb1 for both the systems.

2.2 Transmission Simulations

Transmission simulations were performed by choosing a NbS_2 orthogonal unit cell far from the interfaces as a left lead, followed by one more NbS_2 unit cell, four WSe_2 unit cells, one other NbS_2 unit cells, and finally one NbS_2 orthogonal unit cell as the right lead.

The potential of the left and the right electrodes differ by 40 meV, which we have taken into account by shifting the onsite energies of the right electrodes by 40 meV with respect to the left one.

2.3 Wannierization

For the lead, a NbS_2 unit cell far from the interface was taken. The band structure was first calculated using density function theory (DFT) within the Quantum Espresso package. A tight

binding model was then set up to parametrize this system consists of Nb d and S p states in their basis. The onsite energies and the hopping off-diagonal terms were determined from the interface of Quantum Espresso with Wannier90. Figure S6 shows a comparison of the bandstructure obtained using DFT and wannier for the lead. A good description of the bandstructure was obtained.

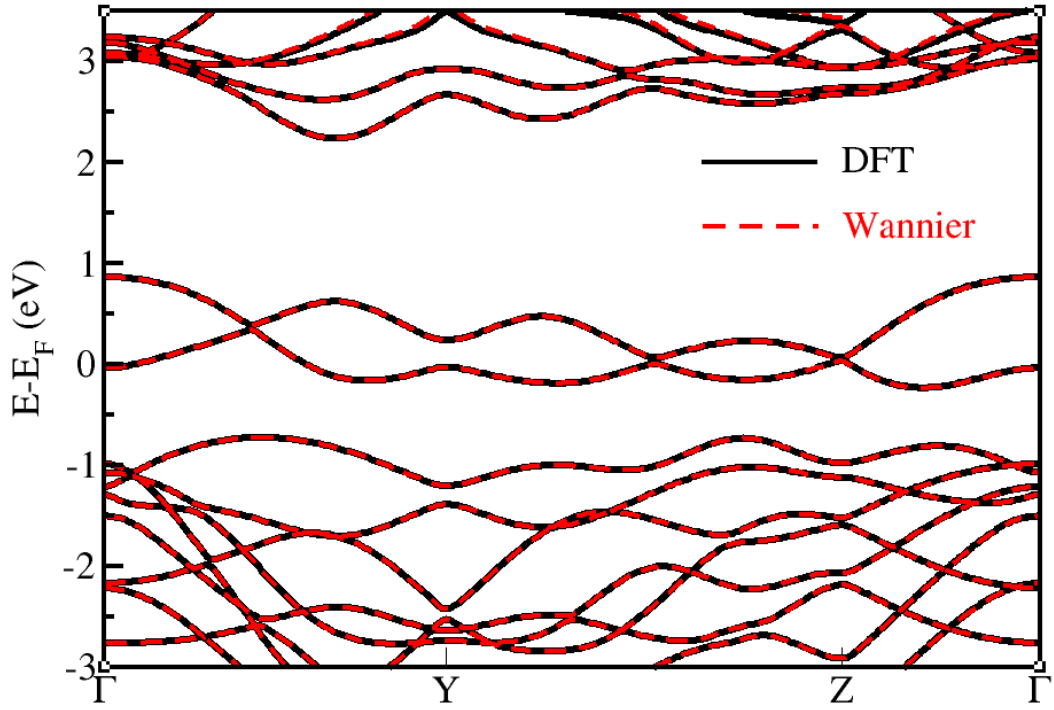

Figure S6: Bandstructure of the lead using DFT (black solid lines) and wannier (red dotted lines) along various symmetry directions.

For the Lateral heterostructure and the defected systems, in the basis set, Nb/W d and S/Se p states were considered. A good description of the bandstructure was obtained in each case. Figure S7, S8 and S9 shows the comparison of bandstructure after wannierization with the one obtained using DFT for the unperturbed system, system with defect in the middle of the semiconducting region and the system with defect at the interface respectively.

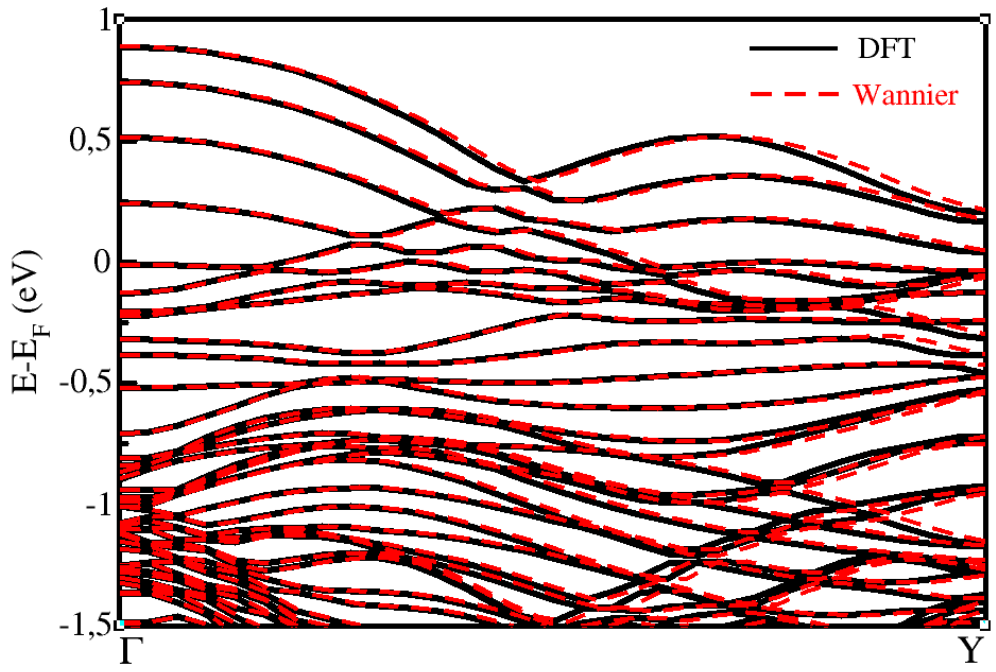

Figure S7: Bandstructure of the unperturbed using DFT (black solid lines) and wannier (red dotted lines) along Gamma to Y direction of the Brillion zone.

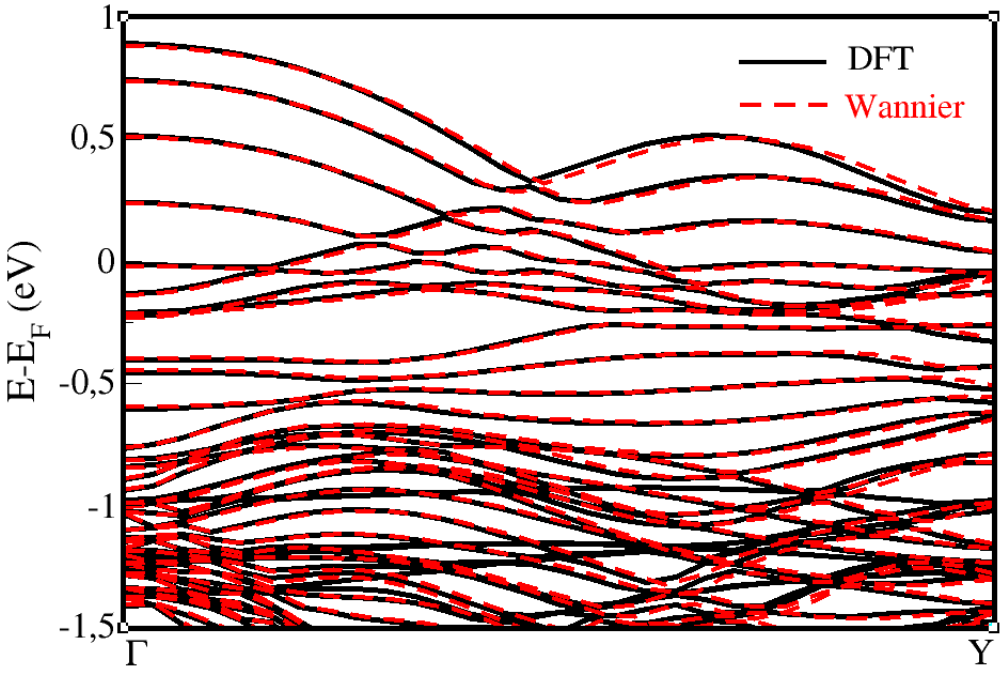

Figure S8: Bandstructure of the perturbed system where the middle of the semiconducting region was perturbed, using DFT (black solid lines) and wannier (red dotted lines) along Gamma to Y direction of the Brillion zone.

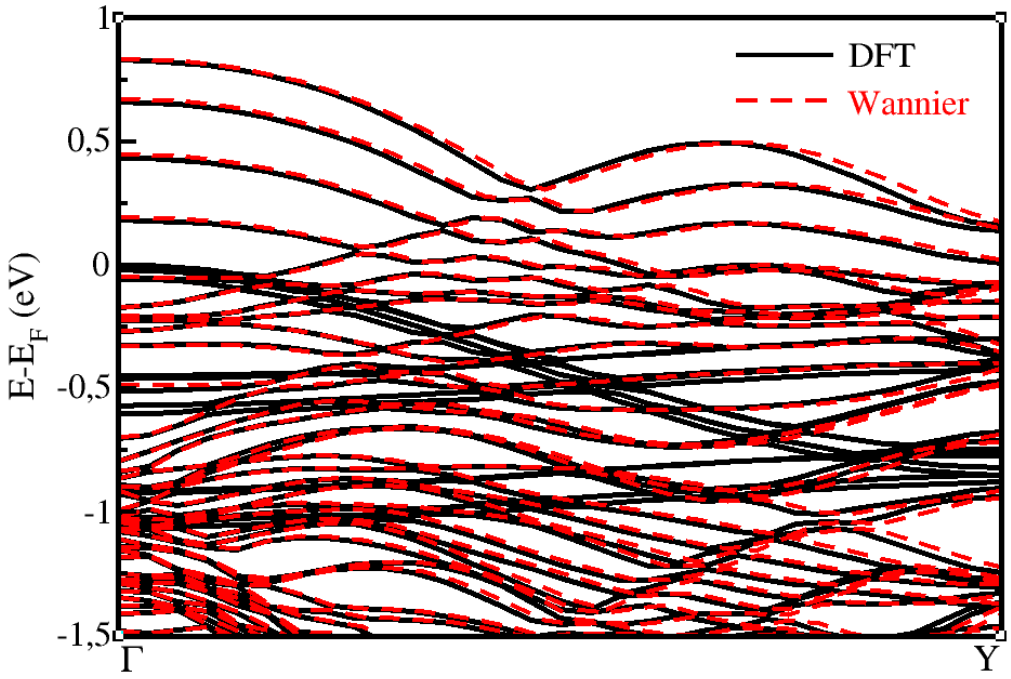

Figure S9: Bandstructure of the perturbed system where the interfaces were perturbed, using DFT (balck solid lines) and wannier (red dotted lines) along Gamma to Y direction of the Brillion zone.

Note: There are a few bands around the Fermi level in the bandstructure obtained using DFT is not present in the wannier bandstructure in S9 as these bands have their origin from LI and F states, whereas in the wannier basis only Nb/W d and S/Se p states were used.

2.4 Density of States of the semiconductor region.

We analyze the potential profiles of the three systems following the procedure prescribed in [2], where from the unperturbed system (Figure S10 a) we take the fragment of far from the interface (Figure S10b) and using its density of state (DOS) (Figure S10 c) and the potential profile of each of the system we understand the transmission profile of each system.

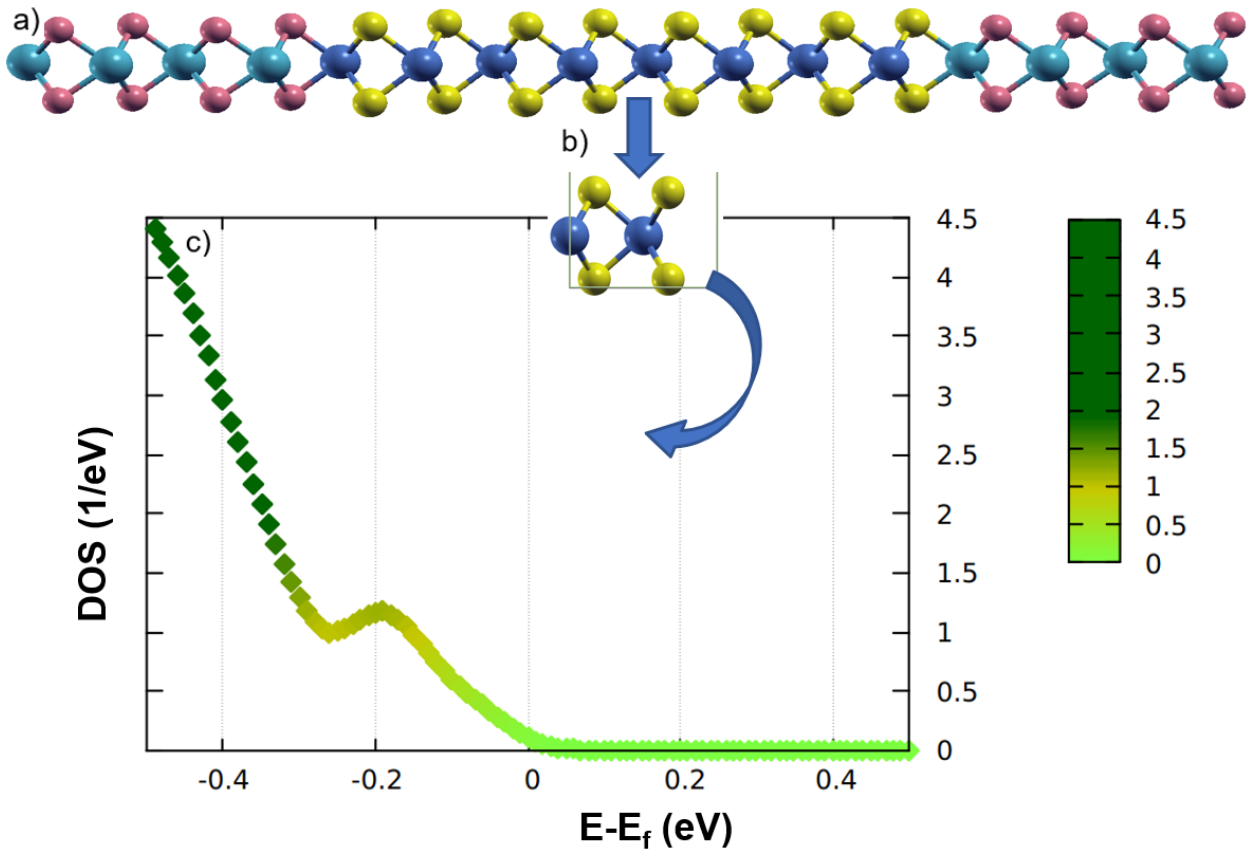

Figure S10 a): The NbS_2/WSe_2 unperturbed system. b) WSe_2 fragment far from the interface and its c) DOS where the dark color of the bar represents higher DOS and lower color represents lower DOS.

2.5 LDOS of W and Se in the semiconductor region.

We analyze the LDOS of W and Se atoms from the monolayer and use it to understand the decrease/increase of transmission in the defected systems compared to the unperturbed system. Figure S11 b) shows the transmission profiles of the unperturbed system (purple) and the defected system (red) shown in Figure S11 a). Figure S11c) shows LDOS of W and Se atoms from the semiconducting regions for the unperturbed system and Figure S11d) shows LDOS of W and Se atoms from the semiconducting regions for the defected system, where the defect is placed in the middle of the semiconducting region. We can see that there is a decrease in the density of states of W4 atom as we go from the unperturbed system to the defected one, as a result there is a decline in the transmission. It can also be seen that the Se LDOS are not significant in the energy window where transmission profile is calculated. Similar analysis was

done for the system with defect at the interface and is shown in Figures S11 e) - S11 g). Figure S11e) shows the transmission profile of the unperturbed system(purple) along with the defected one (red) shown in Figure S11h). Figure S11f) shows the LDOS of W and Se atoms for the unperturbed system and S11g) shows the LDOS for the defected system.

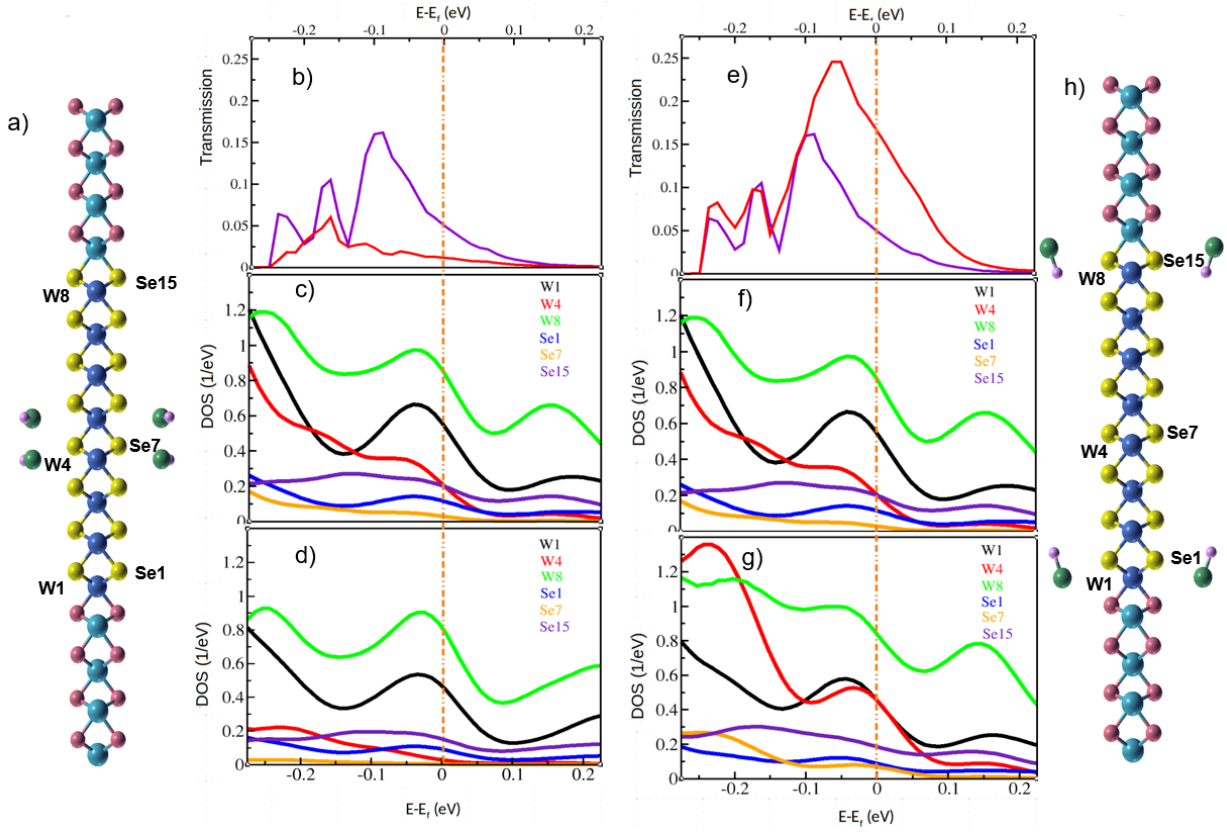

Figure S11 a): System with defect in the middle of the semiconducting region. b) Transmission profiles of the unperturbed (purple) system and for the system shown in S11 a). c) LDOS of W and Se atoms in the unperturbed system. d) LDOS of W and Se atoms in the defected system shown in S11a). e) Transmission profiles of the unperturbed system (purple) and for the system shown in S11h). f) LDOS of W and Se atoms in the unperturbed system. g) LDOS of W and Se atoms in the defected system shown in S11h)

References

[1]: Saunders, V.R.; Freyria-Fava, C.; Dovesi, R.; Salasco, L.; Roetti, C. On the electrostatic potential in crystalline systems where the charge density is expanded in Gaussian functions. *Molecular Physics* **1992,** 77, 629-665.

[2]: Golsanamlou, Z. ; Sementa, L. ; Cusati, T. ; Iannaccone, G. ; Fortunelli, A. Theoretical Analysis of a 2D Metallic/Semiconducting Transition-Metal Dichalcogenide NbS_2//WSe_2 Hybrid Interface. *Adv. Theory Simul*. **2021**, 4, 2100164.